Development and Laboratory Testing of a Lightning Current Measurement System for Wind Turbines

F. Vukovic, V. Milardic, D. Milos, B. Filipovic-Grcic, N. Stipetic, B. Franc

***Abstract*--Dimensioning, testing and maintenance of the lightning protection system of wind turbines can be improved using the local distributions of lightning current parameters instead of those on which lightning protection standards rely. This paper presents a prototype system for measuring lightning currents' waveforms on wind turbines. The prototype is being developed at the Faculty of Electrical Engineering and Computing, University of Zagreb, Croatia. The system's fundamental components are two Rogowski coils and their corresponding integrators. One coil is optimized for lower frequencies and amplitudes, while the other is for higher ones. The cRIO real-time controller is used as an acquisition system, with acquisition logic developed using LabVIEW. The controller has one digitizer for each coil and a GPS synchronization module. The system was tested in the High Voltage Laboratory at University. It was recently installed on an actual wind turbine in Croatia, located in an area characterized by high winter lightning activity. Simultaneously with the prototype measurement system, the lightning activity in the wind turbine micro-location will be monitored by three other systems: the lightning location system, additional lightning monitoring sensors installed in the blades of the same wind turbine and a high-speed camera installed at the wind turbine location.**

***Keywords*: acquisition system, LabVIEW, lightning current measurement, Rogowski coils, wind turbines.**

I. Introduction

In light of the relatively high susceptibility of wind turbines (WTs) to atmospheric discharges and their growing integration into power systems, special attention must be given to the dimensioning of the lightning protection system (LPS) in order to reduce the number of faults and downtimes. Standard IEC 62305-1:2010 [1] specifies how to design and dimension components of LPS according to lightning current parameters: peak current (I), average steepness of the current ($\mathrm{d}i/\mathrm{d}t$), total charge transfer (Q), specific energy content (W/R) and duration (T). The standard defines four lightning protection levels (LPL) of LPS. Each level has a defined set of maximum values for lightning current parameters, representing the upper limits above which the physical integrity of LPS components is compromised. This set of maximum values of lightning current parameters is adopted by IEC 61400-24:2019 [2], the standard for lightning protection of wind energy systems.

The issue with the lightning current parameters that both standards rely on in the dimensioning of LPS is that they were obtained based on the measurements conducted in Switzerland on two instrumented towers [3], [4]. Those measurements were done on high, static towers instead of WTs. They reflect parameters of local lightning currents, which do not represent lightning current waveshapes for all other areas and might not be applicable elsewhere. IEC 61400-24:2019 acknowledges this issue as Q during winter lightning in Japan may exceed 1000 C, well over the IEC LPL I limit of 300 C [5].

Most currently active systems for measuring lightning currents are installed on high, static structures such as telecommunication or meteorological towers. They are present all around the world in countries such as Austria [6], Germany [7], Switzerland [8], Canada [9], Brazil [10], Japan [11] and China [12]. On the other hand, measurement systems installed on WTs are not as present worldwide as those installed on high and static objects. Up to these days, the development of systems for measuring lightning currents on WTs has been in Japan. Lightning current measurements on wind turbines have been conducted in Japan using single Rogowski coils as early as 2002, which amounts to approximately 20 years of experience. The five-year-long NEDO (New Energy and Industrial Technology Development Organization) project in Japan represented the most extensive research on measuring lightning strikes to wind turbines [13]. The project lasted from 2008 to 2013. During the project, a Rogowski coil was installed at 27 wind turbines at the base of their towers, and 21 of 27 wind turbines were in the winter lightning area. Additionally, Mitsubishi Heavy Industries, Ltd. (MHI) started to measure lightning strikes in 2002 by installing two Rogowski coils on a 600 kW WT. In 2005 MHI expanded the measurements to 37 wind turbines across Japan [14]. Finally, Electric Power Development Co., Ltd., known as J-Power, measures lightning strikes in the Nikaho wind farm using Rogowski coils [14]. A Rogowski coil is installed at the base of three WTs [15]. An additional measurement system based on Rogowski coils can be found in [16]. The system described in [16] has two Rogowski coils of different frequency and amplitude ranges for measuring lightning currents on WTs. Both coils are installed at the transition between the hub and nacelle, which is, in practice, an area of limited accessibility and unfavorable operating conditions (possible interference

This work was partly supported by the Croatian Science Foundation and the European Regional Development Fund within project DESMe, KK 01.1.1.07.0028.

F. Vukovic, V. Milardic, D. Milos, B. Filipovic-Grcic, N. Stipetic and B. Franc are with the Faculty of Electrical Engineering and Computing, University of Zagreb, Croatia (e-mail: franjo.vukovic@fer.hr).

Paper submitted to the International Conference on Power Systems Transients (IPST2023) in Thessaloniki, Greece, June 12-15, 2023.

with other equipment, vibrations etc.).

In Croatia, almost all WTs are installed in the coastal area. Croatia's coastal region has great wind potential but is hilly and, according to the winter lightning world map in [2], characterized by medium to high winter lightning activity. Thus, a high percentage of upward lightning may be expected. That may lead to many lightning strikes with Q surpassing the IEC LPL I limit of 300 C. Considering these facts, it is vital to investigate the local lightning currents' waveshapes in order to determine local distributions of I, di/dt, Q, W/R and T.

II. Lightning Current Measurement System

The measurement system consists of two current sensors and a real-time controller. Both sensors are Rogowski coils connected to an integrator via a coaxial cable, and they were custom-made based on specified requirements by an experienced manufacturer. They are different in terms of current and frequency ranges for which they are optimized. The first sensor is a high-frequency and high-current sensor, while the second sensor is optimized for lower current amplitudes and frequencies. Real-time controller cRIO is used for digitizing, timestamping and storing the information obtained by the sensors. It utilizes three modules to accomplish previously listed tasks: two digitizers, one for each sensor, and a GPS synchronization module. The controller's exact modules are a high-speed digitizer, a low-speed digitizer and a GPS synchronization module. Fig. 1. shows a schematic illustration of the prototype measurement system intended for installation on WTs.

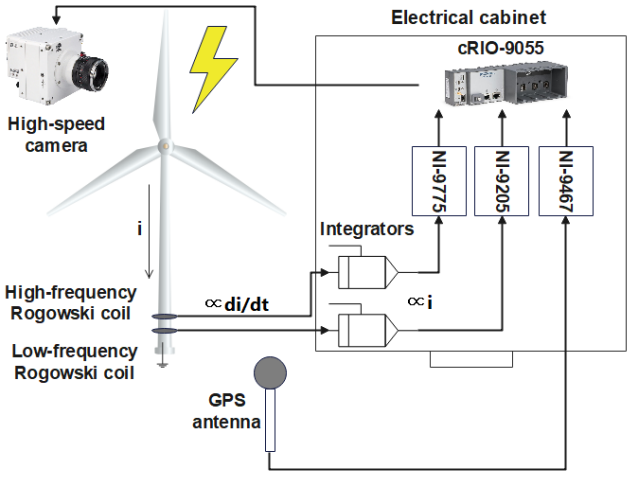

Fig. 1. Lightning current measurement system for wind turbines

Rogowski coils encircle the base of a WT to detect the lightning current flowing through the tower. Their output voltage is proportional to the time derivative of the lightning current. The coils are connected to the integrators to reconstruct the lightning current signal. The voltage signals on the integrators' outputs are proportional to the lightning current and are directly connected to the real-time controller. The integrators and the real-time controller are mounted together in an electrical cabinet. The high-speed digitizer acquires data from the high-frequency sensor and, as such, has a sampling rate of up to 20 MHz. On the other hand, a low-speed digitizer acquires data from the low-frequency sensor, and its sampling rate can only go up to 250 kHz. The GPS synchronization module is connected to the GPS antenna to synchronize the real-time controller to GPS time in order to provide precise timestamps for the acquired lightning current measurement.

A. Characteristics of the Current Sensors

The current sensors were custom-made due to the requirement for an unusually large circumference, which had to fit the WT base. Both sensors have the same physical characteristics, the circumference of their Rogowski coils of 13.5 m and the length of the coaxial cables for integrators' connection of 6.2 m. Regarding electrical characteristics, the high-frequency sensor has a frequency range from 0.2 Hz to 1 MHz and a current range of ±250 kA. It is optimized to measure fast return strokes and superimposed impulses that can occur on initial continuous currents (ICCs). ICCs are a feature of upward lightning. The low-frequency sensor has a frequency range from 0.05 Hz to 10 kHz and a current range of ±12.5 kA. This sensor is aimed at measuring ICCs. Table I gives the electrical specifications for both sensors.

TABLE I
Electrical Characteristics of the Sensors

Specifications	**High-frequency sensor**	**Low-frequency sensor**
High frequency, -3dB (kHz)	1000	10
Low frequency, -3dB (Hz)	0.2	0.05
Peak current limit for correct measurement (kA)	±250	±12.5
Peak di/dt limit for effective measurement (kA/µs)	200	1
Peak di/dt limit above which sensor damage occurs (kA/µs)	200	200
Integrator saturation limit (kA)	±250	±250
Sensitivity (mV/A) – calibrated at 50 Hz	0.03	0.6
Peak output (V)	±7.5	±7.5
Noise (mV_{p-p})	10	20
DC offset (mV)	±2	±5
Droop (%/ms)	0.22	0.06

As seen in Table I, currents in the range of ±250/±12.5 kA at the input of sensors are transformed to ±7.5 V voltage range at the output of the integrators. Hence, both digitizers of the acquisition system receive voltage signals proportional to lightning currents in the ±7.5 V voltage range.

B. Acquisition System

The cRIO is a real-time embedded industrial controller consisting of an Intel Atom dual-core microprocessor and an Artix-7 FPGA module and offers four slots for C series modules. This project utilizes three C series modules: high-speed digitizer, low-speed digitizer and GPS synchronization module. Moreover, cRIO has two Gigabit Ethernet ports, a USB 3.1 host port, a USB 2.0 device port and a MicroSD card slot.

The high-speed digitizer is a 4-channel digitizer with a 14-bit ADC resolution and ±10 V nominal input range. It can measure samples up to 20 MS/s/channel and store them in its

128 Mbit onboard memory. In this application, only one channel is used. Hence, the maximum possible sampling frequency is 20 MHz. This module digitizes the output signals of the high-frequency sensor. The output of the integrator of the high-frequency sensor is connected to the high-speed digitizer input channel using a coaxial cable.

The low-speed digitizer is a 32-channel digitizer with an aggregated sampling frequency of 250 kHz. It has a 16-bit ADC resolution. The input range is flexible and can be set between ±0.2 V, ±1 V, ±5 V or ±10 V. In this project, ±10 V has been chosen as the input range to match the output of the integrator. The low-speed digitizer acquires and digitizes data from the low-frequency sensor. The integrator output is connected to the low-speed digitizer input channel with a coaxial cable.

The GPS synchronization module synchronizes the Artix-7 FPGA of the real-time controller with International Atomic Time (TAI) to enable accurate timestamping of lightning strike events based on the arrival of a pulse per second (PPS) signal. The GPS module is connected to the GPS antenna.

The data acquired by the digitizers is stored locally on the 32 GB MicroSD card. The communication with the controller is realized through one of its Gigabit Ethernet ports to enable the remote fetching of the lightning strike data stored on the MicroSD card.

C. LabVIEW Application and Acquisition Parameters

The data acquisition application for the cRIO was developed in LabVIEW. The application contains the implementation of triggering logic of the digitizers, time synchronization to an external source (GPS), time stamping and saving acquired data locally to the MicroSD card. The cRIO has an Artix-7 FPGA with a 40 MHz onboard clock that offers high-speed execution of logic needed to trigger digitizers on time and generate precise timestamps when triggers occur. The 40 MHz onboard clock generates accurate timestamps every 25 ns. The accuracy of the synchronization of the controller with the GPS time is approximately ±100 ns. Both digitizers are set to be triggered when input signals exceed a specific absolute value and remain above it for a certain time, i.e., for a specified number of samples termed as stable samples. The triggers of both digitizers are independent, and the trigger moments of both digitizers receive GPS timestamps. Based on those timestamps, it is possible to determine the precise absolute time of every pre-sample and sample of the high-speed and low-speed digitizer records. Currently, the controller separately stores data recorded with the high-speed and low-speed digitizer, which can be correlated and overlapped according to the GPS timestamps.

The acquisition parameters of both digitizers can be changed anytime by remotely modifying the application input file. It is possible to specify trigger levels, sampling frequencies, number of stable samples, number of pre-samples and the total number of samples for each digitizer separately. Defining the sampling frequency and the total number of samples implicitly specifies the duration of the record of the digitizers. Table II shows the current settings of the acquisition system for the WT.

TABLE II
CURRENT SETTINGS OF THE ACQUISITION SYSTEM

Acquisition parameters	**High-speed digitizer**	**Low-speed digitizer**
Sample rate (kHz)	10000	30
Trigger level (V)	0.075	0.025
Number of stable samples	1	1
Total number of samples	15000	60000
Number of pre-trigger samples	1500	6000

As seen from the table, the high-speed digitizer sampling frequency is set to 10 MHz and the total number of samples to 15000. That means that the total duration of its record is 1500 µs. The number of pre-samples is 10% of the total number of samples. Furthermore, the trigger level is set to 0.075 V. Considering the sensitivity of the high-frequency sensor of 0.03 mV/A, the digitizer is triggered when the lightning current exceeds 2500 A. It is possible to successfully record 32 such records before the data must be transferred from the digitizer to the real-time controller. The data transfer then causes a dead time of around 2 s. For the low-speed digitizer input parameters, the sampling frequency is set to 30 kHz and the total number of samples to 60000. Considering the specified sampling frequency and the total number of samples, the total duration of the low-speed digitizer record is 2 s. The trigger level is set to 0.025 V. The trigger occurs when the lightning current exceeds 41.67 A.

III. LABORATORY TESTING

The measurement system was assembled and tested in the High Voltage Laboratory (HVL) at the Faculty of Electrical Engineering and Computing, University of Zagreb [17], [18]. The industrial electrical cabinet of 500×500×210 mm was used to mount the real-time controller with its modules and the integrators. The GPS antenna connected to the GPS module inside the assembled cabinet was installed on the roof of the laboratory building. Several types of tests were conducted to verify the functionality of both the sensors and the acquisition system.

A. Real-time Controller Testing Results

A signal generator integrated into a digital oscilloscope was used to generate signals for the digitizers to verify the functionality and accuracy of the developed LabVIEW application. Various functions of the cRIO were verified, such as the digitizers' trigger condition and the GPS timestamping of the trigger moment. Various voltage signals of different frequencies and amplitudes were generated as inputs for both digitizers.

Fig. 2. illustrates the time correlation of high-speed and low-speed digitizer records of the same event by overlapping the records using their GPS timestamps. A square wave signal with a minimum amplitude of -1 V and a maximum amplitude of 3 V was generated using the oscilloscope. Its rise time was 1 µs, and its positive peak duration was 100 ms. It was successfully simultaneously recorded by both digitizers.

The triggers of both digitizers were set to 1.5 V. The high-speed digitizer sampling frequency was set to 10 MHz and the

record duration to 10 ms. The low-speed digitizer sampling frequency was 30 kHz, and the total duration of the record was 2 s. In the upper graph of Fig. 2, the time axis range is 2 s to illustrate the whole duration of the low-speed digitizer record. As seen from the upper graph, the two independent records overlap well. The legend gives the GPS timestamps of the beginning of the records. In the lower graph of Fig. 2, the rising part of the signal is zoomed for a better view of the high-speed digitizer record since its duration is only 10 ms.

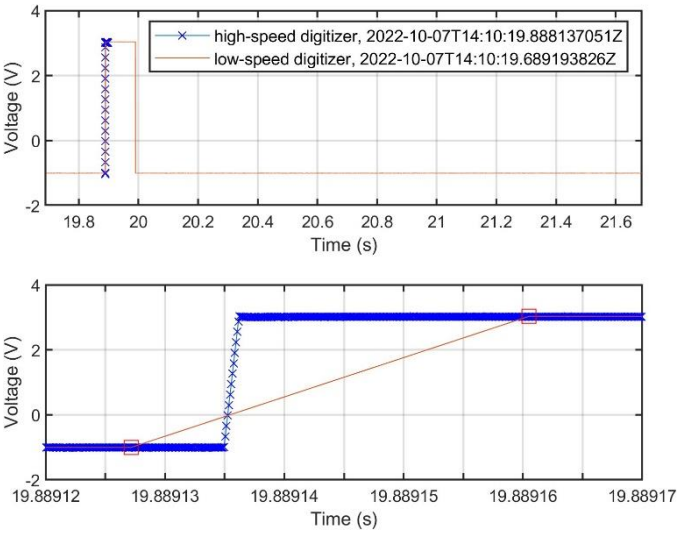

Fig. 2. Time correlation of low-speed and high-speed digitizer records of the same event

As seen from the lower graph, the low-speed digitizer with the sampling frequency of 30 kHz missed the rising portion of the square signal since the rise time was only 1 µs. Meanwhile, the high-speed digitizer frequency was high enough (10 MHz) to capture several points on the rising portion of the signal. In conclusion, both digitizers adequately recorded the same input signal according to their specified acquisition parameters. Furthermore, their records were successfully correlated using GPS timestamps.

B. Sensor Testing Results

Several 8/20 µs current impulses of different amplitudes were generated in the HVL to test the low-frequency and high-frequency current sensors. Fig. 3 shows the test circuit for 8/20 µs current impulse generation to test the sensors. Sensors were tested one by one. In this case, sensors were tested separately from the acquisition system. Hence, the integrators were connected directly to one of the oscilloscope's measuring channels. The surge currents were generated by charging the capacitor bank using high voltage rectified by the diode. The capacitor was discharged through the spark gap into the second part of the circuit. The generated current impulse was then simultaneously measured by two systems: by one of the current sensors that were tested and by a shunt resistor. Because of the laboratory equipment limitation to generate currents of adequately high amplitudes, Rogowski coils of both sensors were coiled around the conductor through which impulse current flows. Several turns were formed to achieve the equivalent required current amplitude for a single turn.

Four 8/20 µs current impulses ranging from approximately 3 to 5 kA were generated to test the low-frequency sensor. The low-frequency sensor had two turns. That means the equivalent currents ranged from 6 to 10 kA. Table III provides measurement results of the low-frequency sensor and the shunt resistor. Measurements results show that amplitudes measured by the low-frequency sensor are always higher than the same amplitudes measured by the shunt resistor. The maximum difference between the low-frequency sensor and shunt measurement was approximately 10.5%. This difference is probably caused partially by the sensor's frequency response in the high-frequency range and partially by the influence of the current loop and corresponding parasitic capacitances.

Five 8/20 µs current impulses in the range of 3 to 7 kA were produced to test the high-frequency sensor. The high-frequency sensor had four turns. That means the equivalent currents ranged from 12 to 28 kA. Table IV lists the high-frequency sensor and the shunt measurements. The results lead to the same conclusion as before. The amplitudes measured by the high-frequency sensor are always higher than the same amplitudes measured by the shunt resistor. The maximum difference between the high-frequency sensor and the shunt measurement was approximately 13.4%. A difference between these measurement results is expected. It can be attributable partly to the fact that current amplitudes from the sensor were determined using the transfer factor from calibration at 50 Hz and partly to the fact that the sensor had four turns, which resulted in parasitic capacitances. Test results with high current impulse could be used for determining transfer factors in the high-frequency range.

Fig. 4 illustrates a low-frequency and shunt measurement of 8/20 µs impulse current (Table III, meas. no. 4). As seen in the figure, the waveform measured by the low-frequency sensor lags the waveform measured by the shunt resistor. The lag is probably caused by the limited frequency range of the low-frequency sensor, which only goes up to 10 kHz.

TABLE III
COMPARISON BETWEEN THE LOW-FREQUENCY SENSOR AND SHUNT MEASUREMENTS OF 8/20 µS IMPULSE CURRENTS

Meas. no.	Sensor (kA) transfer factor at 50 Hz	Shunt (kA)	Difference (%)
1.	4.03	3.65	10.49
2.	5.47	5.22	4.71
3.	3.95	3.68	7.40
4.	5.20	4.82	7.88

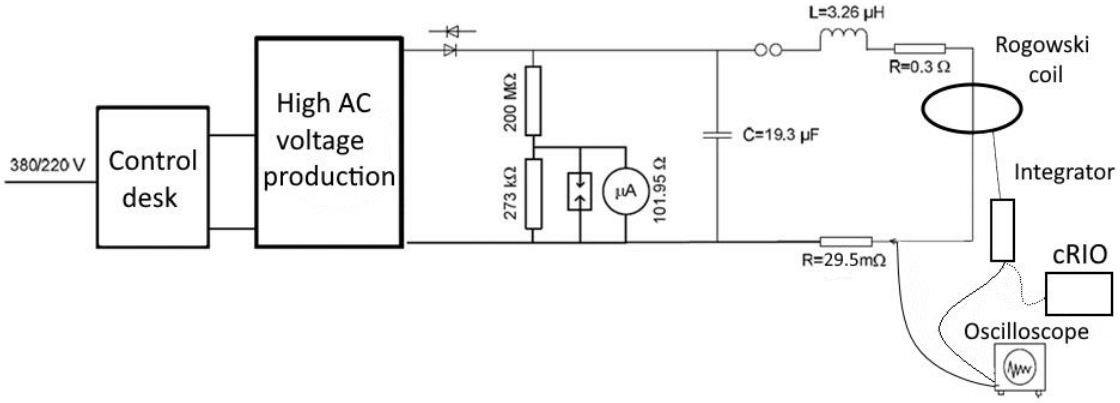

Fig. 3. Test circuit for evaluating the performance of the prototype measurement system

TABLE IV
COMPARISON BETWEEN THE HIGH-FREQUENCY SENSOR AND SHUNT MEASUREMENTS OF 8/20 µS IMPULSE CURRENTS

Meas. no.	Sensor (kA) transfer factor at 50 Hz	Shunt (kA)	Difference (%)
5.	4.17	3.71	12.45
6.	5.50	4.85	13.38
7.	8.17	7.39	10.56
8.	6.83	6.20	10.10
9.	8.25	7.39	11.64

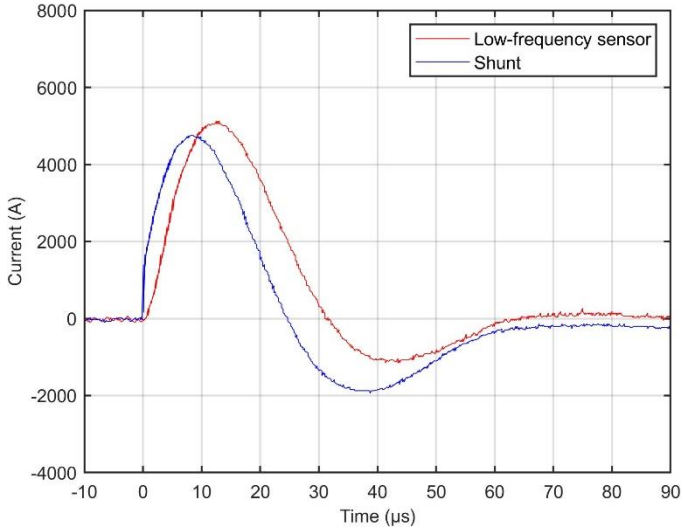

Fig. 4. Waveforms of measurement no. 4. The low-frequency sensor measured an amplitude of 5.20 kA (transfer factor from 50 Hz calibration), while the shunt measured 4.82 kA.

C. Overall System Testing Results

The last phase of laboratory measurements covered testing the overall system's functionality. The same test setup was used as before (Fig 3.). In this case, instead of connecting the integrator output to the oscilloscope, it was connected to the corresponding digitizer of the cRIO real-time controller. The high-frequency sensor was connected to the high-speed digitizer of the cRIO. The high-frequency Rogowski coil was set to have five turns. The low-frequency sensor and its corresponding digitizer were not tested since it was not possible to generate an appropriate low-frequency current.

Several 8/20 µs current impulses with amplitudes ranging from 1 to 10 kA were generated. Since the high-frequency Rogowski coil had five turns, equivalent currents ranged from 5 to 50 kA. The generated impulse currents were simultaneously measured by the 29.5 mΩ shunt resistor connected to the oscilloscope and by the high-frequency Rogowski coil connected to the real-time controller.

Table V summarizes the results of both the prototype system and shunt resistor measurements, with the calculated difference between the two measurements. The results demonstrate two things. Firstly, amplitudes measured by the prototype system are always higher than the simultaneous shunt measurements. This overshoot may be happening because the sensors are calibrated for 50 Hz. Secondly, the difference between measurements lowers as the current amplitude rises. The high-frequency sensor is optimized for a wide current amplitude range, and the measurement error is higher at lower currents. The table shows the most significant difference is approximately 17.1%, while the lowest is 13%.

Fig. 5 shows the waveforms of measurement no. 13. According to the figure, the waveform measured by the high-frequency sensor and cRIO almost perfectly follows the waveform measured by the shunt. Unlike the low-frequency sensor measurement (Fig. 4), there is no lag in this case because the high-frequency sensor frequency range goes up to 1 MHz.

TABLE V
COMPARISON BETWEEN MEASUREMENTS OF 8/20 µS IMPULSE CURRENTS WITH THE HIGH-FREQUENCY SENSOR CONNECTED TO THE CRIO AND SHUNT RESISTOR

Meas. no.	Prototype (kA) – transfer factor at 50 Hz	Shunt (kA)	Difference (%)
1.	1.37	1.17	17.09
2.	2.19	1.90	15.26
3.	2.99	2.61	14.56
4.	2.98	2.62	13.74
5.	3.81	3.31	15.11
6.	4.61	4.06	13.55
7.	5.44	4.77	14.05
8.	6.26	5.47	14.44
9.	7.08	6.20	14.19
10.	8.00	7.05	13.48
11.	8.82	7.73	14.10
12.	9.65	8.54	13.00
13.	10.49	9.25	13.41

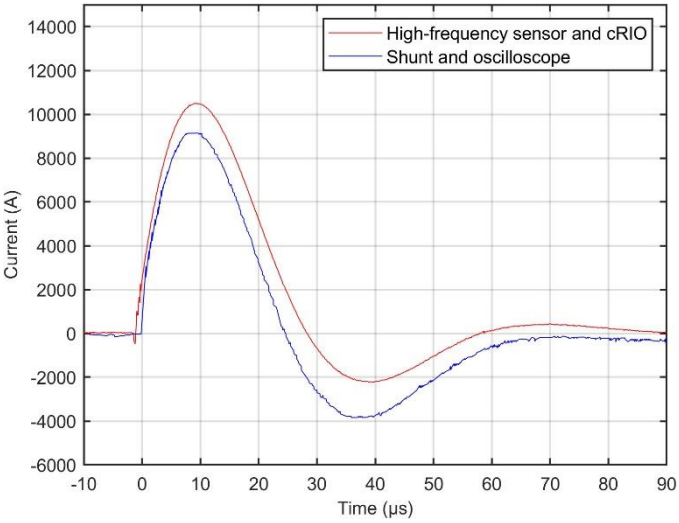

Fig. 5. Waveforms of measurement no. 13. The prototype system measured an amplitude of 10.49 kA, while the shunt measured 9.25 kA.

In summary, the sensors were tested only with high 8/20 μs current impulses of different amplitudes. The testing can be expanded to high-current impulses not only of different amplitudes but also of different frequencies in order to obtain transfer factors in the high-frequency range that can be used to correct on-site measurements.

IV. Installation and Plans for Validation in a Real Environment

The lightning measuring system was recently installed on a WT in wind farm (WF) WF Voštane, located in an area with significant winter lightning activity. The WF consists of 14 WTs, each having a rated power of 3 MW. The WT for the prototype measurement system was selected based on two things. First, it is located at the highest altitude compared to other WTs in the WF. Second, after the WF installation in 2013., the lightning strike density around the chosen WT increased 5.25 times [19], representing the most significant increase in the considered area. The chosen WT is situated 1265 m above sea level. Its tower is 80 m high, and the blades are 49 m long. The maximal structure height when one blade is aligned with the tower is 132 m.

The installation of the measurement system also included the establishment of a communication infrastructure to enable remote monitoring and control of its operation. The measuring system has been continuously operating since the installation, with exceptions when it was reset several times due to a change of acquisition parameters to adjust the digitizers' record lengths and trigger levels. Several lightning strikes have already been measured. Two independent systems confirmed those lightning events: the lightning location system (LLS) and the lightning monitoring system installed in the blades. The obtained measurements have expected waveforms and are the first proof of the prototype system's functionality. The waveforms are currently under analysis and will be used to optimize the acquisition settings and improve the application.

A. Comparison with LM-S Lightning Monitoring System

As mentioned before, the commercially available lightning monitoring system (LM-S) was installed on the WT together with the prototype measuring system. The LM-S detects lightning strikes and determines lightning current parameters. Its operation is based on a magneto-optic phenomenon known as the Faraday effect. The system consists of three sensors, each placed in one blade and connected to the evaluation unit via a fiber optic cable. The evaluation unit contains algorithms for time and the lightning current parameters calculation, but it does not record the current waveform. The parameters are recorded in the lightning log, which can be fetched remotely. The time of the lightning strike and the lightning current parameters determined by the LM-S system can then be compared with the parameters calculated from the lightning current waveform measured by the sensors and the cRIO. The LM-S sensitivity starts at 5 kA. Therefore, it is not expected to record strikes with lower amplitudes, such as ICC. In addition, this system cannot confirm the multiplicity of lightning flashes because it gives only one timestamp and one value of each lightning current parameter, no matter how many lightning strokes are in a lightning flash. Nevertheless, this system will serve as event confirmation and for comparison of lightning current parameters for a significant portion of strikes with amplitudes higher than 5 kA.

B. Comparison with Lightning Location System

Croatia's LLS is a part of the European lightning detection network (LINET). There are six LINET sensors installed in Croatia. LLS provides information on the location, time, amplitude, polarity and type of lightning strikes regarding the inter-cloud and cloud-ground classification. Based on the LLS data and the definition of the attraction area from [2], automatic weekly reports are generated to continuously monitor the lighting activity in the WF area and the chosen WT micro-location. Up to now, the attraction area definition is well-defined since the number of strikes within the attraction area correspond to those recorded by the prototype system. The LLS data also serve as event confirmation and, aside from exact timestamp comparison, enables the comparison of the strike's multiplicity, amplitude and polarity.

C. High-speed Camera

Phantom VEO 1310 high-speed camera will be installed in the substation, about 3.5 km from the WT. It will be used to visually confirm all lightning strikes to the WT by providing a video recording of the event. Based on the high-speed video, it will be possible to determine whether the strike was upward or downward and the exact point of the strike. Therefore, it is expected that the slow-motion records will assist in differentiating strikes to the hub from the ones to the blades and upward from downward strikes. The camera records will be the only confirmation for measured ICC cases. The camera will be GPS synchronized. Its GPS timestamps will be compared to the timestamps of all other monitoring systems.

The camera is still being tested in the HVL. Fig. 6 shows the high-speed camera in HVL aimed at the insulator in order

to record the flashover phenomenon.

Fig. 6. High-speed camera testing in the HVL

Fig. 7 illustrates the electrical breakdown process in the air between two rods separated approximately 30 cm. The left electrode was grounded while the high AC voltage was applied to the right electrode. The voltage was gradually increased until the complete electrical breakdown of the air occurred. The resolution was set to 640 x 360 and the speed to 39000 fps. The time interval between the two consecutive frames was 25.6 µs. A total of 6 frames of the whole video are shown. In the first two frames, initial leader development is visible. In the third frame, the complete electrical breakdown of the air between two electrodes occurred, and an electrical arc was formed. The last three frames show the gradual fading of the electrical arc.

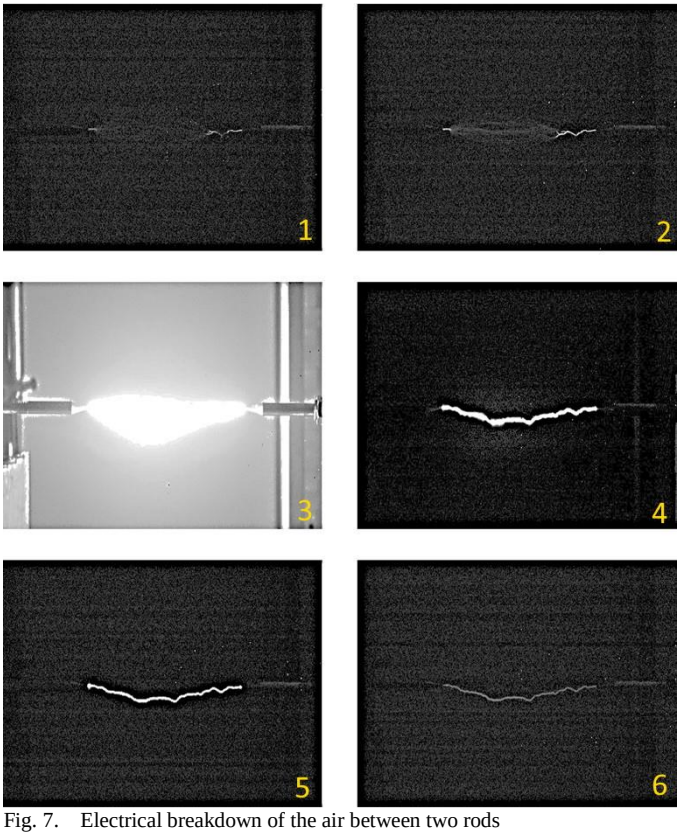

Fig. 7. Electrical breakdown of the air between two rods

Future work includes integrating the high-speed camera into the prototype measurement system. When the prototype measurement system detects lightning current, the real-time controller will send a trigger to the camera to obtain visual proof of the lightning strike (Fig. 1).

V. Conclusions and Future Work

This paper presents a prototype for measuring lightning current waveforms on WTs. From the measured lightning current waveforms, it is possible to determine the distributions of lightning current parameters characteristic for a particular WT location and use it to optimize the dimensioning and the maintenance of LPS.

The measuring system consists of two current sensors. Both sensors consist of a Rogowski coil connected to an integrator. One sensor is optimized to measure lower frequency and lower amplitude strikes, while the other is optimized to measure higher frequency and higher amplitude strikes. The cRIO real-time controller with two digitizers and a GPS synchronization module is used for acquisition purposes.

The prototype was tested at the Faculty of Electrical Engineering and Computing, University of Zagreb, in the High Voltage Laboratory. It was recently installed on an actual WT in Croatia. The system has been in continuous operation since installation, it is remotely monitored, and the first measurements showed expected and promising results.

Further work includes installing a high-speed camera at the substation near the WT and analyzing and comparing all lightning activity recorded by all mentioned monitoring systems. Based on this analysis, the acquisition settings of the prototype measurement system and the high-speed camera will be optimized to capture efficiently as much information on the lightning activity as possible. Furthermore, the waveforms measured by the prototype measurement system will be processed by filtering frequencies that are out of the frequency range of sensors, particularly the ones that are close to the resonant frequencies of the coils. The impact of wave reflections from the ground and blade tips will be numerically eliminated from the measured lightning current waveforms.

VI. References

[1] *Protection Against Lightning—Part 1: General Principles*, IEC Standard 62305-1, Dec. 2010.

[2] *Wind energy generation systems—Part 24: Lightning protection*, IEC Standard 61400-24, July 2019.

[3] K. Berger, R. B. Anderson, and H. Kroninger, "Parameters of lightning flashes," *Electra*, vol. 41, pp. 23–37, 1975.

[4] R. B. Anderson, and A. J. Eriksson, "Lightning parameters for engineering application," *Electra*, no. 69, pp. 65-102, 1980.

[5] K. Miyake, T. Suzuki and K. Shinjou, "Characteristics of winter lightning current on Japan Sea Coast," *IEEE Transactions on Power Delivery*, vol. 7, no. 3, pp. 1450-1457, July 1992.

[6] N. Watanabe, A. Nag, G. Diendorfer, H. Pichler, W. Schulz, V. A. Rakov, and H. K. Rassoul, "Characteristics of Currents in Upward Lightning Flashes Initiated From the Gaisberg Tower," *IEEE Transactions on Electromagnetic Compatibility*, vol. 61, no. 3, pp. 705-718, June 2019.

[7] F. H. Heidler, and C. Paul, "High-Speed Video Observation, Currents, and EM-Fields From Four Negative Upward Lightning to the Peissenberg Tower, Germany," *IEEE Transactions on Electromagnetic Compatibility*, vol. 63, no. 3, pp. 803-810, June 2021.

[8] M. Azadifar, M. Rubinstein, F. Rachidi, V. A. Rakov, G. Diendorfer, W. Schulz, and D. Pavanell, "A Study of a Large Bipolar Lightning Event Observed at the Säntis Tower," *IEEE Transactions on Electromagnetic Compatibility*, vol. 61, no. 3, pp. 796-806, June 2019.

[9] S. Kazazi, A. M. Hussein, and P. Liatos, "Evaluation of the performance characteristics of the North American Lightning Detection Network based on recent CN Tower lightning data," *2015 International Symposium on Lightning Protection (XIII SIPDA)*, pp. 327-333, Sept. 2015.

[10] S. Visacro, M. Guimarães, P. Mattioli, and M. H. Murta Vale, "Features of Upward Lightning Measured in a Tropical Region and Their Potential to Cause Hazardous Effects," *IEEE Transactions on Electromagnetic Compatibility*, vol. 61, no. 3, pp. 745-750, June 2019.

[11] T. Miki, M. Saito, T. Shindo, and M. Ishii, "Current Observation Results of Downward Negative Flashes at Tokyo Skytree From 2012 to 2018," *IEEE Transactions on Electromagnetic Compatibility*, vol. 61, no. 3, pp. 663-673, June 2019.

[12] Z. Qiu, Y. Yang, Z. Qin, M. Chen, F. Lyu, H. Guo, Y. Du, Y. Gao, G. Zhang, and S. Wang, "Optical and Current Measurements of Lightning Attachment to the 356-m-High Shenzhen Meteorological Gradient Tower in Southern Coastal Area of China," *IEEE Access*, vol. 7, pp. 155372-155380, Oct. 2019.

[13] M. Saito, and M. Ishii, "Characteristics of return strokes associated with upward lightning flashes observed in winter," *2018 34th International Conference on Lightning Protection (ICLP)*, pp. 1-5, 2018.

[14] Y. Ueda, S. Arinaga, M. Fukuda, N. Iwai, T. Matsushita, and K. Inoue, "Measurement Experience of Lightning Currents to Wind Turbines," Mitsubishi Heavy Industries, Ltd. Technical Review, vol. 44, no. 4, pp. l-6, Dec. 2007.

[15] K. Michishita, S. Yokoyama, and N. Honjo, "Measurement of Lightning Current at Wind Turbine Near Coast of Sea of Japan in Winter," *IEEE Transactions on Electromagnetic Compatibility*, vol. 61, no. 3, pp. 807-814, June 2019.

[16] J. Birkl, T. Böhm, G. Diendorfer, F. Heidler, C. Paul and H. Pichler, "Measurement of lightning currents on high structures and wind turbines," *2018 34th International Conference on Lightning Protection (ICLP)*, Rzeszow, Poland, 2018, pp. 1-8.

[17] Faculty of Electrical Engineering and Computing, University of Zagreb, High Voltage Laboratory website: https://www.fer.unizg.hr/lvn

[18] DESME project website: https://desme.fer.hr/desme/en

[19] N. Stipetic, B. Filipovic-Grcic, I. Uglesic, and A. Tokic, "Investigation of direct lightning strikes to wind turbine blades," International Conference on Power System Transients (IPST), Perpignan, France, June 2019.